

Free space millimeter wave-coupled electro-optic high speed nonlinear polymer phase modulator with in-plane slotted patch antennas

D. H. Park,^{1,2,*} V. R. Pagán,^{1,2} T. E. Murphy,² J. Luo,³ A. K.-Y. Jen,³ and W. N. Herman¹

¹Laboratory for Physical Sciences, College Park, Maryland 20740, USA

²Dept. of Electrical and Computer Engineering, University of Maryland, College Park, Maryland 20742, USA

³Dept. of Materials Science and Engineering, University of Washington, Seattle, Washington 98195, USA

*leomac@lps.umd.edu

Abstract: We report in-plane slotted patch antenna-coupled electro-optic phase modulators with a carrier-to-sideband ratio (CSR) of 22 dB under an RF power density of 120 W/m² and a figure of merit of 2.0 W^{-1/2} at the millimeter wave frequencies of 36-37 GHz based on guest-host type of second-order nonlinear polymer SEO125. CSR was improved more than 20 dB by using a SiO₂ protection layer. We demonstrate detection of 3 GHz modulation of the RF carrier. We also derive closed-form expressions for the modulated phase of optical wave and carrier-to-sideband ratio. Design, simulation, fabrication, and experimental results are discussed.

©2015 Optical Society of America

OCIS codes: (060.5060) Phase modulation; (060.5625) Radio frequency photonics; (130.5460) Polymer waveguides.

References and links

1. J. Capmany and D. Novak, "Microwave photonics combines two worlds," *Nat. Photonics* **1**(6), 319–330 (2007).
2. T. R. Clark and R. Waterhouse, "Photonics for RF Front Ends," *IEEE Microw. Mag.* **12**(3), 87–95 (2011).
3. V. R. Pagán, B. M. Haas, and T. E. Murphy, "Linearized electrooptic microwave downconversion using phase modulation and optical filtering," *Opt. Express* **19**(2), 883–895 (2011).
4. T. E. Dillon, C. A. Schuetz, R. D. Martin, S. Shi, D. G. Mackrides, and D. W. Prather, "Passive millimeter wave imaging using a distributed aperture and optical upconversion," *Proc. SPIE* **7837**, 78370H (2010).
5. F. T. Sheehy, W. B. Bridges, and J. H. Schaffner, "60 GHz and 94 GHz Antenna-Coupled LiNbO₃ Electrooptic Modulators," *IEEE Photon. Technol. Lett.* **5**(3), 307–310 (1993).
6. Y. N. Wijayanto, H. Murata, and Y. Okamura, "Electrooptic Millimeter-Wave-Lightwave Signal Converters Suspended to Gap-Embedded Patch Antennas on Low-*k* Dielectric Materials," *IEEE J. Sel. Top. Quantum Electron.* **19**(6), 3400709 (2013).
7. G. A. Lindsay and K. D. Singer, eds., *Polymers for Second-Order Nonlinear Optics* (ACS Symposium Series 601, 1995).
8. W. N. Herman, S. R. Flom, and S. H. Foulger, eds., *Organic Thin Films for Photonic Applications* (ACS Symposium Series 1039, 2010).
9. X. Zhang, B. Lee, C. Lin, A. X. Wang, A. Hosseini, and R. T. Chen, "Highly Linear Broadband Optical Modulator Based on Electro-Optic Polymer," *IEEE Photon. J.* **4**(6), 2214–2228 (2012).
10. X. Zhang, A. Hosseini, X. Lin, H. Subbaraman, and R. T. Chen, "Polymer-Based Hybrid-Integrated Photonic Devices for Silicon On-Chip Modulation and Board-Level Optical Interconnects," *IEEE J. Sel. Top. Quantum Electron.* **19**(6), 3401115 (2013).
11. X. Zhang, A. Hosseini, S. Chakravarty, J. Luo, A. K.-Y. Jen, and R. T. Chen, "Wide optical spectrum range, subvolt, compact modulator based on an electro-optic polymer refilled silicon slot photonic crystal waveguide," *Opt. Lett.* **38**(22), 4931–4934 (2013).
12. S. Inoue and A. Otomo, "Electro-optic polymer/silicon hybrid slow light modulator based on one-dimensional photonic crystal waveguides," *Appl. Phys. Lett.* **103**(17), 171101 (2013).
13. B. Bortnik, Y.-C. Hung, H. Tazawa, B.-J. Seo, J. Luo, A. K.-Y. Jen, W. H. Steier, and H. R. Fetterman, "Electrooptic Polymer Ring Resonator Modulation up to 165 GHz," *IEEE J. Sel. Top. Quantum Electron.* **13**(1), 104–110 (2007).
14. H. Huang, S. R. Nuccio, Y. Yue, J. Yang, Y. Ren, C. Wei, G. Yu, R. Dinu, D. Parekh, C. J. Chang-Hasnain, and A. E. Willner, "Broadband Modulation Performance of 100-GHz EO Polymer MZMs," *J. Lightwave Technol.* **30**(23), 3647–3652 (2012).
15. M. Lee, H. E. Katz, C. Erben, D. M. Gill, P. Gopalan, J. D. Heber, and D. J. McGee, "Broadband Modulation of Light by Using an Electro-Optic Polymer," *Science* **298**(5597), 1401–1403 (2002).

16. B. Li, J. Vemagiri, and R. Dinu, "Design and Modeling of Traveling-Wave Electro-Optic Polymer Modulator for Ultrahigh Speed Applications," *J. Lightwave Technol.* **27**(5), 606–611 (2009).
17. X. Zhang, A. Hosseini, H. Subbaraman, S. Wang, Q. Zhan, J. Luo, A. K.-Y. Jen, and R. T. Chen, "Integrated Photonic Electromagnetic Field Sensor Based on Broadband Bowtie Antenna Coupled Silicon Organic Hybrid Modulator," *J. Lightwave Technol.* **32**(20), 3774–3784 (2014).
18. O. D. Herrera, K.-J. Kim, R. Voorakaranam, R. Himmelhuber, S. Wang, V. Demir, Q. Zhan, L. Li, R. A. Norwood, R. L. Nelson, J. Luo, A. K.-Y. Jen, and N. Peyghambarian, "Silica/Electro-Optic Polymer Optical Modulator with Integrated Antenna for Microwave Receiving," *J. Lightwave Technol.* **32**(20), 3861–3867 (2014).
19. D. Park, Y. Leng, J. Luo, A. Jen, and W. N. Herman, "High speed electro-optic polymer phase modulator using an in-plane slotline RF waveguide," *Proc. SPIE* **7936**, 793607 (2011).
20. R. Song, H. C. Song, W. H. Steier, and C. H. Cox III, "Analysis and Demonstration of Mach-Zehnder Polymer Modulators Using In-Plane Coplanar Waveguide Structure," *IEEE J. Quantum Electron.* **43**(8), 633–640 (2007).
21. M. Born and E. Wolf, *Principles of Optics*, 7th ed. (Cambridge University, 1999).
22. C. A. Balanis, *Antenna Theory*, 3rd ed. (Wiley-Interscience, 2005)
23. EOSPACE[®] Inc. website. http://www.eospace.com/phase_modulator.htm
24. T. Hirano, K. Okada, J. Hirokawa, and M. Ando, "60 GHz On-Chip Patch Antenna Integrated in a 0.18- μm CMOS Technology," in *Proceedings of IEEE International Symposium on Antennas & Propagation (IEEE, 2012)*, pp. 62–65.
25. J. Luo and A. K.-Y. Jen, "Highly Efficient Organic Electrooptic Materials and Their Hybrid Systems for Advanced Photonic Devices," *IEEE J. Sel. Top. Quantum Electron.* **19**(6), 3401012 (2013).
26. Y. N. Wijayanto, H. Murata, and Y. Okamura, "Electro-optic microwave-lightwave converters utilising quasi-phase-matching array of patch antennas with gap," *Electron. Lett.* **48**(1), 36–38 (2012).
27. V. R. Almeida, Q. Xu, C. A. Barrios, and M. Lipson, "Guiding and confining light in void nanostructure," *Opt. Lett.* **29**(11), 1209–1211 (2004).
28. R. W. Ridgway, J. A. Conway, and C. L. Dohrman, "Microwave Photonics: Recent Programs at DARPA," in *Proceedings of IEEE International Topical Meeting on Microwave Photonics (IEEE, 2013)*, pp. 286–289.
29. G.-K. Chang and C. Liu, "1-100GHz microwave photonics link technologies for next-generation WiFi and 5G wireless communications," in *2013 International Topical Meeting on Microwave Photonics (IEEE MWP, 2013)*, pp. 5–8.

1. Introduction

Radio-over-fiber (RoF) systems have been particularly attractive for relaying microwave to millimeter wave (mm-wave) radio frequency (RF) signals compared with using prohibitively lossy coaxial cables [1–3]. An EO phase modulator with an integrated antenna is promising for photonic RF front-ends in modern wireless communication systems because it is cost-effective and compact. A passive millimeter wave imaging technique has been reported using an array of horn antennas directly connected to electro-optic (EO) modulators [4]. Several antenna-integrated EO modulators (EOM) based on nonlinear crystal materials such as LiNbO_3 or LiTaO_3 have been studied [5,6]. Poled polymers based on second-order nonlinearities have been widely studied for potential applications such as modulators and resonators [7–12]. Advantages of utilizing nonlinear polymers in EOM include relatively low refractive index with little dispersion, large second-order nonlinearity, and broad bandwidth. EO modulation up to 165 GHz has been demonstrated using traveling wave polymer modulators [13–15]. Indeed, a 100 Gbps polymeric DP-QPSK modulator has been developed by Gigoptix, Inc [16]. Bowtie antenna-integrated polymeric phase modulators operating at 10–15 GHz have recently been reported [17,18]. The design and fabrication of an antenna-coupled optical phase modulator must achieve (1) low optical loss, (2) single optical mode, (3) velocity match, (4) high poling efficiency, (5) high antenna gain, and (6) high conversion efficiency from RF to optical phase shift [6,16,19,20]. Careful consideration of the integrated antenna design is crucial because the RF performance, including bandwidth and gain, directly affects the device's RF-induced optical phase shift. Dipole and patch antenna structures are possible for planar integration with the optical waveguide [5,6]. However, the dipole antenna structure has a smaller antenna effective area and is not easily impedance-matched to coplanar transmission lines. On the other hand, a slotted patch antenna structure can be integrated in-plane with an optical ridge waveguide without the need for a coplanar transmission line and impedance matching. Unlike the coplanar structures reported in Refs [5]. and [6], the in-plane structure provides better EO polymer poling efficiency and higher overlap factor resulting in higher optical phase modulation [19,20]. The in-plane electric field induced in the gap of the

slotted patch by the incident RF radiation produces optical phase modulation resulting from a change in refractive index of the nonlinear waveguide.

In this paper, we demonstrate devices consisting of a free space coupled antenna integrated with an EO high speed phase modulator (HSPM) operating at mm-wave frequencies of 36-37 GHz for photonic RF front-ends in wireless communication systems, based on a second-order nonlinear polymer in-plane waveguide structure. Our best device exhibited a CSR of 22 dB under an RF power density of 120 W/m^2 and we compare this device with the case of a device having no SiO_2 protection layer. Here, we define the CSR as the ratio of the optical power in the optical carrier to that of the first-order sideband. This protection layer deposited on substrates enables poling the nonlinear polymer waveguide at higher poling fields by blocking leakage currents. We present mathematical expressions for the optical phase modulation and CSR for comparison with experimental results. We discuss the design, simulation, fabrication, and experimental results for the single and array patch antenna-coupled nonlinear polymer optical waveguide devices and propose a figure of merit (FOM) for evaluating the performance of this type of device. We also demonstrate optical detection of 3 GHz modulation of the RF carrier signal.

2. Theory

In this section, closed-form analytic expressions for the optical phase modulation induced by the incident RF wave are presented to facilitate the design of optimized patch antenna/array devices. First, we derive analytic expressions for phase modulation of the optical wave for both a single slotted patch antenna and array, and then find the relation between CSR and optical phase modulation. We also propose a figure of merit to describe our device performance.

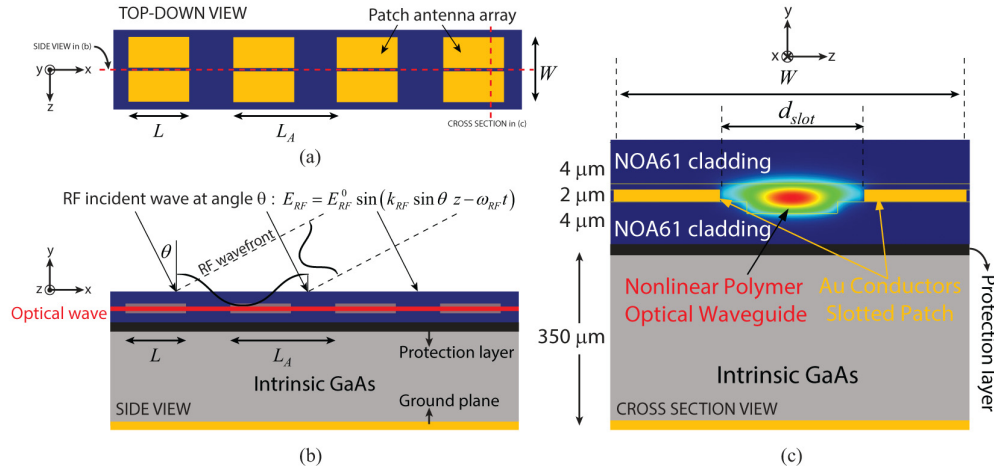


Fig. 1. (Not to scale) (a) Top view of the device; the patch antenna structure with a 4 element array ($N = 4$) is in-plane with an optical waveguide with under the NOA61 top cladding layer. (b) Side view of the device along the center cut-line shown in (a) showing incident RF plane waves. The layer in black is a SiO_2 protection layer on an intrinsic GaAs substrate to block leakage current through the substrate. (c) Cross section of the device along the vertical cut-line shown in (a) with the simulated fundamental optical mode profile shown in the center. The Ti/Au slotted patch is about $1\text{-}1.2 \mu\text{m}$ thick and the bottom of the substrate is coated with $1\text{-}2 \mu\text{m}$ thick Ti/Au for ground plane of the antenna.

2.1 Optical phase modulation for single patch antenna

Figure 1 shows the schematic of the antenna-integrated phase modulator. Slotted patch antennas is located on the NOA61 bottom cladding layer to be in-plane with the optical waveguide. Consider light propagating a distance L through a material with a time varying and spatially varying refractive index

$$n(x,t) = n_0 + \delta n(x,t), \quad \delta n(x,t) = -\frac{1}{2} n_0^3 r_{33} \Gamma E_{slot}(x,t), \quad (1)$$

where n_0 and r_{33} are the optical effective index and the EO coefficient in the nonlinear materials, respectively [21], and Γ is the overlap factor between the RF and optical fields. A localized RF wave produced by an antenna can be assumed to be a plane wave far from the antenna in its far field regime [22]. The incident RF (polarized in z direction on xy plane of incidence) field from an external source is

$$E_{RF} = E_{RF}^0 \sin(k_{RF} \sin \theta x - \omega_{RF} t), \quad (2)$$

where $k_{RF} = 2\pi/\lambda_{RF}$ and θ is the incident angle of the RF wave. Both optical and RF waves are linearly polarized in the direction parallel to the poling field of the nonlinear polymers. The in-plane patch antenna structure is covered by polymer materials (core and cladding) and the power of the incident RF waves decreases somewhat because of the reflection at the polymer layer. The antenna structure can be fabricated on top of the device as a coplanar structure, but this results in much lower RF-induced electric field and overlap factor as stated in the introduction [20]. Using the TE Fresnel transmission coefficient t_{RF} and ignoring possible effects due to the metal electrodes, we approximate the electric field inside the polymer layer to be

$$E_{RF}^{inside} = t_{RF} \cdot E_{RF} = \frac{2 \cos \theta}{\cos \theta + \sqrt{\epsilon_{RF}} \cos \theta'} E_{RF}^0 \sin(k_{RF} \sqrt{\epsilon_{RF}} \sin \theta' x - \omega_{RF} t), \quad (3)$$

where $\epsilon_{RF} (= n_{RF}^2)$ is the dielectric permittivity of the polymer and θ' is the internal angle of incidence inside the polymer layer. Assuming that the electric field inside the waveguide is uniform, the electric field induced by the incident RF wave inside the slot of the patch antenna is $E_{slot}(x,t) = E_{slot}^0 \sin(k_{RF} \sin \theta x - \omega_{RF} t)$. Here we have used $\sqrt{\epsilon_{RF}} \sin \theta' = \sin \theta$, which follows from Snell's law. Assuming that the patch antenna can be considered to be a combination of many half-wave dipole antennas [22], the electric field induced in the slot of the patch can be estimated to be

$$E_{slot}^0 = 2 \cdot t_{RF} \cdot E_{RF}^0 \frac{W_{eff}}{d_{slot}}, \quad (4)$$

where W_{eff} and d_{slot} are the effective length of the patch antenna [22] and the gap size of the slot, respectively. Note that the RF electric field is enhanced by the factor of $E_{slot}^0/E_{RF}^0 = 2 \cdot t_{RF} \cdot W_{eff}/d_{slot}$ in the slot of the patch. We refer to this quantity as the enhancement factor.

As TE-polarized light propagates the nonlinear material possessing both time and spatially varying refractive index $n(x,t)$ given by Eq. (1), the phase difference between it and a reference light wave propagating through the material with constant refractive index n_0 over a small distance dx is

$$d[\delta\phi(x,t)] = k_{op} \delta n(x,t) dx, \quad (5)$$

where $k_{op} = 2\pi/\lambda_{op}$ and λ_{op} is the optical wavelength in vacuum. To determine the accumulated phase difference, from $x_0 = 0$ at the waveguide input at the entrance of the slotted antenna to the end of the slot, we first note that the phase velocity is

$$v_{op} = \frac{c}{n(x,t)} = \frac{c}{n_0} \frac{1}{1 - \frac{A}{n_0} \sin(k_{RF} \sin \theta \cdot x - \omega_{RF} t)} \approx \frac{c}{n_0}, \quad (6)$$

where we have used Eq. (1) and defined $A \equiv n_0^3 r E_{slot}^0 \Gamma / 2$ and c is the speed of light in vacuum. The second term in the denominator can be dropped because $A/n_0 \ll 1$. The group index, $n_g = n_0 + \omega(dn/d\omega)$, is assumed to be close to the effective index. In fact, we found that using a calculated group velocity instead of Eq. (6) resulted in a difference of less than 1% in the optical modulation. Then a phase front having entered the slot at time t_0 will reach point x in the slot at time $t' \approx (n_0/c)x + t_0$. Using Eq. (5), The total accumulated phase difference over the length L of the antenna is then

$$\delta\phi(t_0) = k_{op} \int_0^L \delta n(x, t'(x)) dx = -k_{op} A \int_0^L \sin(k_{RF} (\sin \theta - n_0)x - \omega_{RF} t_0) dx. \quad (7)$$

Integrating Eq. (7), we get

$$\delta\phi(t_0) = k_{op} AL \operatorname{sinc} \left(k_{RF} u \frac{L}{2} \right) \sin \left(\omega_{RF} t_0 - k_{RF} u \frac{L}{2} \right), \quad (8)$$

where $u \equiv \sin \theta - n_0$ and we have used a trigonometric identity for the difference of two cosines. Note that the phase matching condition, $\sin \theta = n_0$, is not possible because $n_0 > 1$. For normal RF incidence ($\theta = \theta' = 0$), we have the following result for the case of time-varying, but not spatially varying RF wave,

$$\delta\phi(t_0) = k_{op} AL \operatorname{sinc} \left(k_{RF} n_0 \frac{L}{2} \right) \sin \left(\omega_{RF} t_0 + k_{RF} n_0 \frac{L}{2} \right). \quad (9)$$

We also note that Eq. (8) is identical to the phase modulation expression for the case of a conventional EO phase modulator based on a travelling RF wave by replacing $\sin \theta$ in $u(\theta)$ with n_{RF} [5].

2.2 Optical phase modulation for a patch antenna array

For an array of N antenna elements each of length L separated by a distance of L_A as illustrated in Fig. 1(a), Eq. (7) takes the form

$$\delta\phi_N(t_0) = -k_{op} A \sum_{s=0}^{N-1} \int_{sL_A}^{sL_A+L} \sin(k_{RF} u x - \omega_{RF} t_0) dx, \quad (10)$$

recalling that $u \equiv \sin \theta - n_0$. Performing the integration and using trigonometric identities gives

$$\delta\phi_N(t_0) = k_{op} AL \operatorname{sinc} \left(\frac{k_{RF} u L}{2} \right) B_N \sin \left\{ \omega_{RF} t_0 - k_{RF} \frac{u [L + (N-1)L_A]}{2} \right\}, \quad (11)$$

where the scaling factor B_N is given in Eq. (24). The details of the derivation are provided in Appendix A. For a single element, that is, $N = 1$, Eq. (11) reduces to Eq. (8). Wijayanto *et al.* have also investigated simulation of phase modulation by numerical integration over distance [6], but their result does not describe angle-dependency for the single patch antenna structure and we have found it to not agree with our experimental results.

2.3 Carrier-to-sideband ratio

The phase-modulated optical signal is assumed to be

$$E = E_{op} e^{j[\omega_{op}t + m \sin(\omega_{RF}t)]}, \quad (12)$$

where m is the modulation depth corresponding to the coefficient of sine in Eq. (11). Using the Jacobi-Anger expansion in Eq. (12) gives

$$E = E_{op} e^{j\omega_{op}t} \left[J_0(m) + \sum_{s=1}^{\infty} J_s(m) e^{js\omega_{RF}t} + \sum_{s=1}^{\infty} (-1)^s J_s(m) e^{-js\omega_{RF}t} \right], \quad (13)$$

where J_s is the s^{th} Bessel function. Note that the first term on the right hand side of Eq. (13) corresponds to the optical carrier component and the last two terms represent the first-order ($s = 1$) and higher order ($s \geq 2$) sidebands. Therefore, the CSR of the first-order sideband can be expressed as

$$\text{CSR} = \left[\frac{J_0(m)}{J_1(m)} \right]^2 = \left[20 \log \frac{J_0(m)}{J_1(m)} \right]_{\text{dB}}. \quad (14)$$

In practice, the modulation depth is $m \ll 1$ and we can use $J_1(m)/J_0(m) \approx m/2$ to further simplify Eq. (14) to

$$\text{CSR} \approx \frac{4}{m^2} = \left[20 \log \frac{2}{m} \right]_{\text{dB}}. \quad (15)$$

For the case of a single and N -element array antenna, the CSR in dB is

$$\text{CSR [dB]} \approx 20 \log \left[\frac{2}{k_{op} AL \sin c \left(\frac{k_{RF} u L}{2} \right) B_N} \right], \quad (16)$$

where the modulation depth is given in Eq. (11).

2.4 Figure of merit for antenna-integrated EO modulators

We propose a figure of merit to describe the performance of antenna-integrated EO modulators using device-specific properties. The modulation depth can be defined in terms of the half-wave voltage V_π and the received voltage V_r in the form [3]

$$m = \frac{\pi V_r}{V_\pi} = \frac{\pi \sqrt{2Z_m P_D A_e}}{V_\pi}. \quad (17)$$

where Z_m , P_D , and A_e are the impedance of the modulator, the power density, and the effective area of the receiving antenna, respectively. Assuming no ohmic loss in the antenna and using $A_e = (\lambda^2/4\pi) G_r$, we have an expression containing the product of device specific parameters and applied RF signals in the form

$$m = \pi \left(\frac{\sqrt{2Z_m G_r}}{V_\pi} \right) \left(\sqrt{P_D \frac{\lambda^2}{4\pi}} \right). \quad (18)$$

Defining the left-most parenthesized quantity in Eq. (18) as the FOM of the device gives

$$\text{FOM} [W^{-1/2}] = \frac{\sqrt{2Z_m G_r}}{V_\pi} = \frac{m}{\pi} \sqrt{P_D \frac{\lambda^2}{4\pi}}. \quad (19)$$

For this proposed FOM, a larger value is, of course, better. For a typical high speed EOM (V_π (at 36 GHz) $\approx \sqrt{2} \cdot V_\pi$ (at 1 GHz) = 5.7 V [23]) with a 0-dBi gain antenna, the FOM can be found to be $1.75 W^{-1/2}$.

3. Design, Simulation, and Fabrication

Figure 1(c) shows a cross section view of the device. Good optical waveguide and antenna designs are important for low optical power and high gain operations resulting in high signal-to-noise ratio (SNR) in RoF systems. The resonant RF frequency depends on both the width of the patch antenna and the RF index of the substrate, typically $W \approx \lambda_{RF} / 2\sqrt{\epsilon_{RF}}$ [22], but the HFSS[®] simulator shows that the optimal width for a given RF frequency is higher than $\lambda_{RF} / 2\sqrt{\epsilon_{RF}}$ because the electromagnetic wave exists partly in the air above the device. We chose $W = 1.5$ mm for about 35 GHz operation. By appropriate design of the antenna dimensions, such devices can be designed to operate at frequencies from a few GHz to over 100 GHz, limited by the chip size and limits of lithography. Two different devices are designed, one with only a single patch and the other with a 2-element patch array structure. The length of the single patch antenna was $L_A = 5.36$ mm and the length of the patch in the array structure was $L = 2$ mm, and we used an array of $N = 2$ antennas. The RF electric field from an external source can be expressed as $E_{RF}^0 = \sqrt{2\eta P_D}$, where η is the free space impedance. The external RF source was introduced using a horn antenna, with polarization adjustable for both parallel and perpendicular to the slot. The power density is given as $P_D = P_t \cdot G / 4\pi r^2$, where P_t , G , and r are transmitter power, gain of the horn antenna, and distance between the horn antenna and the patch antenna, respectively. As shown in Fig. 2, the high frequency simulator HFSS[®] shows that the electric field in the slot can be enhanced by a factor of 400-500 over the incident RF electric field. This is comparable to $2W_{eff} / d_{slot}$ from Eq. (4).

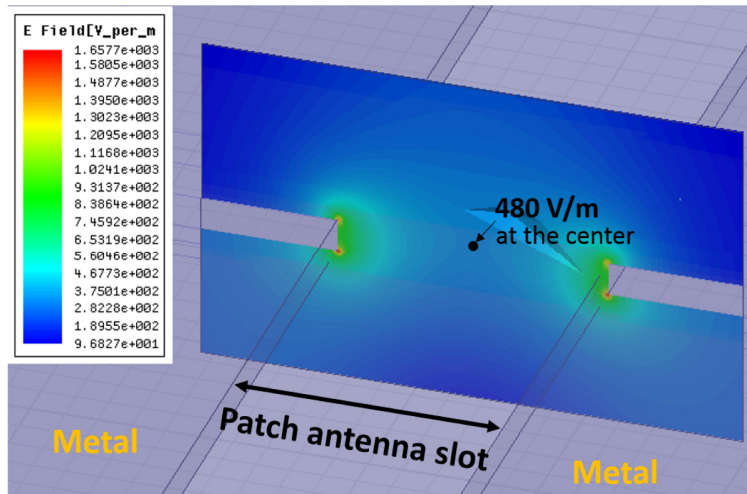


Fig. 2. HFSS[®] Simulation of the magnitude of the electric field in the slot area at normal RF incident wave. The electric field for the RF plane wave is 1 V/m. The highest electric field is 480 V/m in the center of the slot, indicating the enhancement factor is about 480.

An intrinsic GaAs substrate (single-side polished, Wafer Technology Ltd.) is used to minimize leakage current during the poling procedure and to facilitate the dicing procedure to achieve clean facets. As illustrated in Fig. 1(c), a few μm thick insulating layer such as SiO_2 or Si_3N_4 can be grown on the substrate to further avoid the leakage current by plasma-enhanced chemical vapor deposition (PECVD) system (Novellus), because the conductivity of GaAs drastically increases at a poling temperature of 150°C . A $1\text{-}2\ \mu\text{m}$ Au film ground plane for the antenna was e-beam evaporated on the back side of the substrate, as opposed to immediately under the lower optical waveguide cladding layer, in order to increase bandwidth and antenna efficiency due to the thicker antenna substrate [24]. Fused silica or quartz substrate (SiO_2) can be used to increase receiving power caused by low RF index, but it often produces cracked facets after dicing and the spin-coated film on top of it is prone to lift off because of poor adhesion. Unlike the case of LiNbO_3 or LiTaO_3 , additional low- k dielectric material [6] is unnecessary because of the relatively low RF refractive index of nonlinear polymers and cladding materials. A $4\ \mu\text{m}$ thick NOA61 UV curable polymer was spin-cast onto the GaAs substrate and ridge waveguide trenches were patterned on the photo-resist. The patterns were then processed by reactive ion etch (RIE) to get $1\ \mu\text{m}$ deep and $4\ \mu\text{m}$ wide trenches using O_2 gas. The $1.2\ \mu\text{m}$ thick Ti/Au for the slotted patch antenna structure was deposited on the bottom cladding layer using an E-beam evaporator. A trade-off between optical loss by metallic electrodes and V_π in EOM is well-known because the optical field can easily be absorbed by the metal electrode [15,19,20]. The electrode gap used in this work is 8 or $10\ \mu\text{m}$ and the propagation loss is numerically estimated [19] to be less than $5\ \text{dB/cm}$.

A nonlinear polymer thin film, SEO125 [25], was formulated by doping 35-40 wt. % of AJLZ53 to COPS host polymer dissolved in dibromomethane. The solution was filtered with a $0.2\ \mu\text{m}$ -PTFE membrane filter. The nonlinear polymer solution was spin-coated on the patterned bottom cladding with metallic antenna structures to give a $1.8\text{-}2\ \mu\text{m}$ film, thin enough to have a single optical mode. Residual solvent was evaporated after post-baking at 120°C for 5 minutes. The device was further baked at 80°C inside a vacuum oven for over 24 hours and finally another $4\ \mu\text{m}$ top cladding of NOA61 was spin-cast. The slotted patch antenna structure was used as a poling electrode to orient the chromophore molecules in the nonlinear polymer waveguide near the glass transition temperature of 150°C under nitrogen environment. Without a SiO_2 protection layer, a large leakage current up to $10\ \text{mA}$ ($\sim 200 \times 10^3\ \text{A/m}^2$) starts to flow as the temperature increases during the poling procedure. This is because of high conductivity of GaAs substrate near the poling temperature. The current is saturated because of the limitation of power supply. It causes severe voltage drop in the GaAs and the lower cladding. Finally, the device was diced for optical input and output facets and cleaved/diced to remove Ti/Au poling leads.

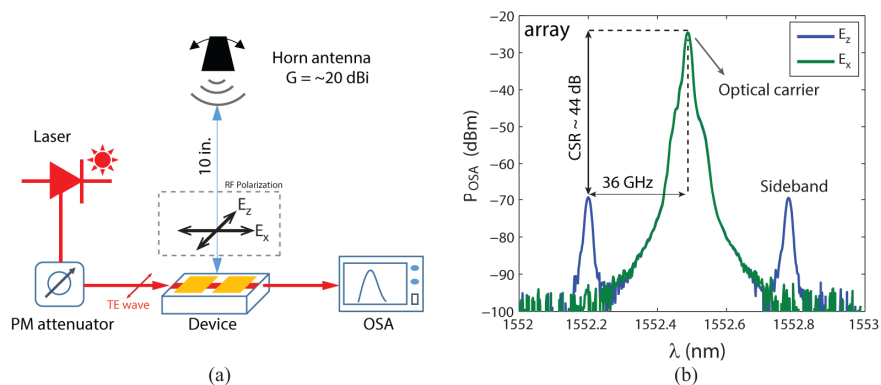


Fig. 3. (a) Schematic of experimental setup. Polarization-maintained attenuator is used to control input power. (b) (Without SiO_2 protection layer) Optical spectra at 36 GHz of the array device. Blue and green lines represent z - and x -polarized RF wave from the horn antenna, respectively.

4. Results

4.1 Without a SiO₂ protection layer

Figure 3(a) shows the experimental setup for characterizing the device. A horn antenna (SH128-20, Fairview Microwave) ranging from 26.5 to 40 GHz with RF amplifier (Agilent N5183A and Microwave Dynamics AP3030-33 amplifier) was used to generate an RF field up to ~50 dBm at the output of the antenna. The RF power density at the device was about 120 W/m². A TE polarized laser beam (1552.5 nm) was launched into the device through a single mode polarization maintaining (PM) fiber and a PM attenuator. Waveguide propagation loss due to absorption, roughness, and the metallic antenna is less than 5 dB/cm for the case of an 8 μm gap. From careful examination of the devices, we believe that most of the substrate light is scattered from the rough surface of the back side of the GaAs substrate. Fiber coupling loss (in/out) is estimated to be 10-15 dB each, because of the loss caused primarily by poor end-facets and mode mismatch. An optical spectrum analyzer (OSA, Yokogawa AQ6370C) was used to observe modulated sidebands around the optical carrier. Figure 3(b) shows clear sidebands for the case of *z*-polarized RF input (parallel to the poling direction) at the mm-wave frequency of about 36 GHz with CSR of 44 dB from the patch antenna array device ($N = 2, L = c/(2n_0 f_{RF})$) poled at 800 V in the 8 μm gap without a SiO₂ protection layer, whereas there is no sideband for the case of *x*-polarized RF input because the *x*-polarized RF wave parallel to the optical waveguide cannot excite an intense electric field inside the slot of the patch antenna.

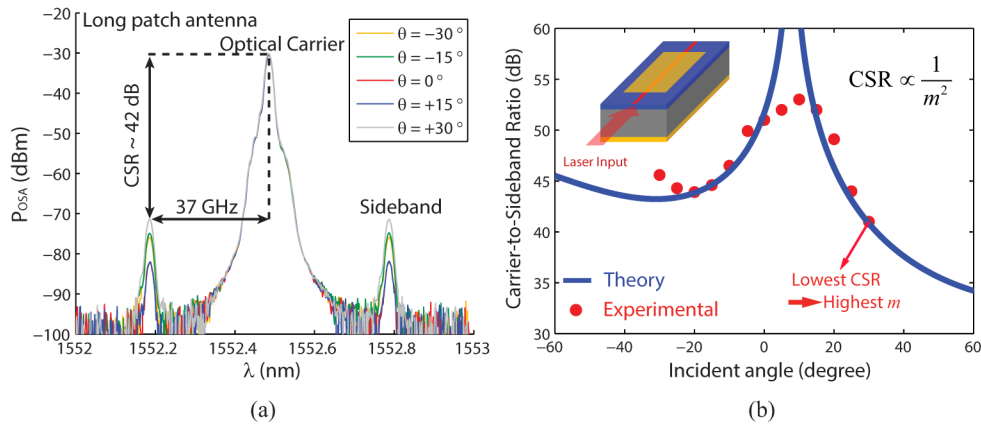


Fig. 4. (Without SiO₂ protection layer) (a) Optical spectra for the single patch antenna at incident angles of -30°, -15°, 0°, 15°, and 30°. (b) CSR as a function of RF incident angle. Red dots are experimental data and the blue line is calculated data based on Eqs. (8) and (15). Note that smaller CSR means higher optical modulation based on Eq. (15).

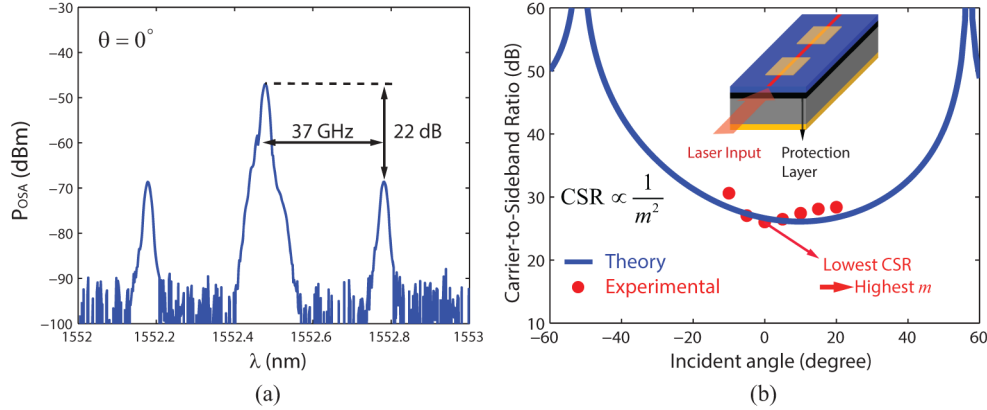


Fig. 5. (With SiO_2 protection layer) (a) Optical spectrum for the array patch antenna at normal incidence showing the best CSR of 22 dB. (b) CSR as a function of RF incident angle. Red dots are experimental data and blue line is calculated data based on Eqs. (11) and (15). The data taken in this experiment was limited by the rotation arm in the setup.

Figure 4(a) shows the experimental results for the 5.359 mm long single patch antenna without a SiO_2 protection layer. The optical modulation varies depending on the index mismatch term $(\sin \theta - n_0)$, as expected from Eq. (11). The length of the patch is twice the optimal length, $c/(n_0 f_{RF})$, so, from Eq. (9), the phase modulation should be zero (infinite CSR) at normal incidence because of destructive interference [5]. However, because of uncertain design parameters such as RF and optical indices, the largest CSR is at $\sim 7^\circ$. As shown in Fig. 4(b), the experimental data show a good agreement with the calculated data based on Eq. (11). ECCOSORB[®] BSR adhesive backed microwave absorbing material was placed on the metal optical table and on parts of the stages to partially suppress reflections, but we believe that the data mismatch around 7° in Fig. 4(b) results from spurious RF reflections in the experimental setup which was not in an anechoic environment. From the data fitting, we were able to make an estimate for the EO coefficient r_{33} of about 10 pm/V with the overlap factor $\Gamma = 0.8$. The low EO coefficient is caused by large leakage current through the substrate resulting in lowering the voltage across the slot area.

4.2 With a SiO_2 protection layer

On the other hand, in case of the device where a SiO_2 protection layer is deposited on a GaAs substrate, CSR was considerably improved by up to 20 dB. Figure 5(a) shows the optical spectrum for the array patch antenna device poled at 750 V in the 10 μm gap. The SiO_2 layer blocks leakage current through the conductive GaAs at high temperatures allowing most of the applied voltage to be applied to the antenna slot without significant voltage loss. This resulted in a poling electric field of 75 V/ μm and a leakage current density of $\sim 20 \text{ A/m}^2$. The estimated EO coefficient r_{33} from the CSR of 22 dB was about 100 pm/V with the overlap factor $\Gamma = 0.8$, suggesting that the SEO125 was optimally poled [25]. The EO coefficient 10 times higher than the case of no protection layer introduces 20 dB improvement in CSR. The CSR of 22 dB under an RF power density of 120 W/m^2 corresponds to 23 dB under 100 W/m^2 . From Eq. (14), the modulation depth corresponding to CSR = 22 dB can be found to be $m = 0.16 \text{ rad}$. Using Eq. (18), a figure of merit (FOM) for this device is estimated to be $2.0 \text{ W}^{-1/2}$, which is comparable to that of a commercially available phase modulator such as the EOSpace[®] 40 GHz EOM attached to a (nonintegrated) 0 dBi antenna. Angle dependent CSR's in Fig. 5(b) show good agreement with simulation. The 3-dB RF bandwidth of an RF device is one of the important parameters in RF communications. As shown in Fig. 6(a), the 3-dB RF bandwidth of our device is about 2 GHz, which allows us to modulate data with the baseband bandwidth of 1 GHz without significant reduction of signal strength. The bandwidth can be

increased more by using a thicker substrate or a high- k substrate, but the high- k material produces a lower enhancement factor because of the shorter patch width at a fixed resonance frequency. In microwave devices, one of the advantages of using low loss substrates is to reduce RF substrate loss at high frequencies [19]. Unlike traveling wave EO modulators, in our devices, most of the incident RF wave is reflected back from the antenna structure except that a small amount of energy is consumed in the metallic antenna and the substrate because there is no transmission line and load. Figure 6(b) shows simulated enhancement factors as a function of frequency when lossless ($\tan\delta = 0$) and lossy ($\tan\delta = 0.0016$ e.g., RO3203) substrates are used. It turns out that no significant change in enhancement factor is observed, but the resonant frequency corresponding to the highest enhancement factor shifts slightly. In fact, devices from Si-doped GaAs ($\rho = 10\text{-}100\ \Omega\cdot\text{cm}$) showed only a 1-2 dB higher CSR than those fabricated on semi-insulating GaAs substrates.

4.3 Modulation of the RF carrier

A simple modulation test was performed to confirm feasibility of wireless RF data transmission through the 2-element patch array device. As shown in Fig. 7(a), we chose to modulate the 36 GHz RF carrier with a sinusoidal modulation frequency of 3 GHz, in order to produce sidebands that could be resolved by our optical spectrum analyzer (Yokogawa®), which had a resolution of 0.02 nm (2.5 GHz). Figure 7(b) shows the optical spectrum with the RF carrier and 3 GHz sinusoidal input. When the RF carrier is modulated with a 3 GHz sinusoidal signal, the optical spectrum shows 3 GHz-spaced sidebands around the RF carrier. Offline deconvolution is performed to recover the original modulation signal as well as both optical and RF carriers, as illustrated in Fig. 7(a). Experimental data (blue) is fitted to multiple Gaussian functions (red). Then, it is deconvolved with the transfer function of the OSA, which is determined simply by the single Gaussian function in the center of the fit representing the optical carrier. The green line in Fig. 7(c) is a deconvolved signal and it shows the recovered impulse signals containing optical and RF carriers, as well as the 3 GHz modulation signal.

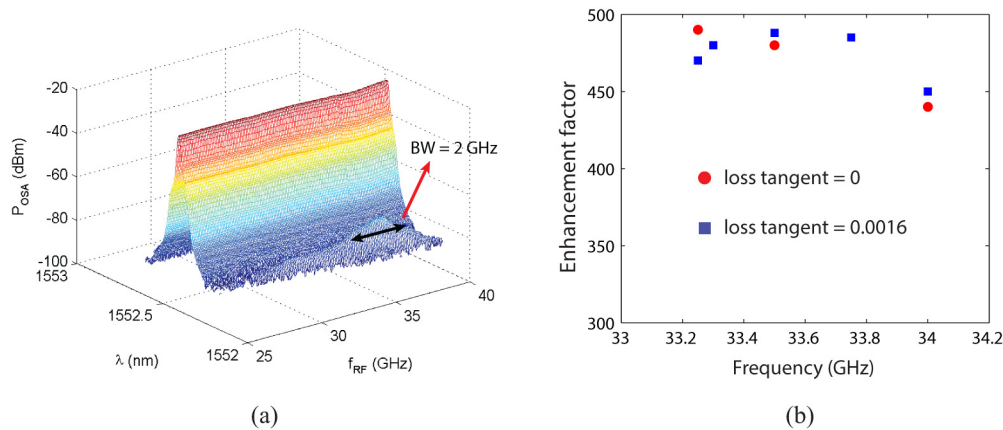


Fig. 6. (a) Optical spectrum as a function of optical wavelength and RF frequency. (b) Simulated enhancement factor as a function of RF frequency in case of lossless and lossy substrate using HFSS®.

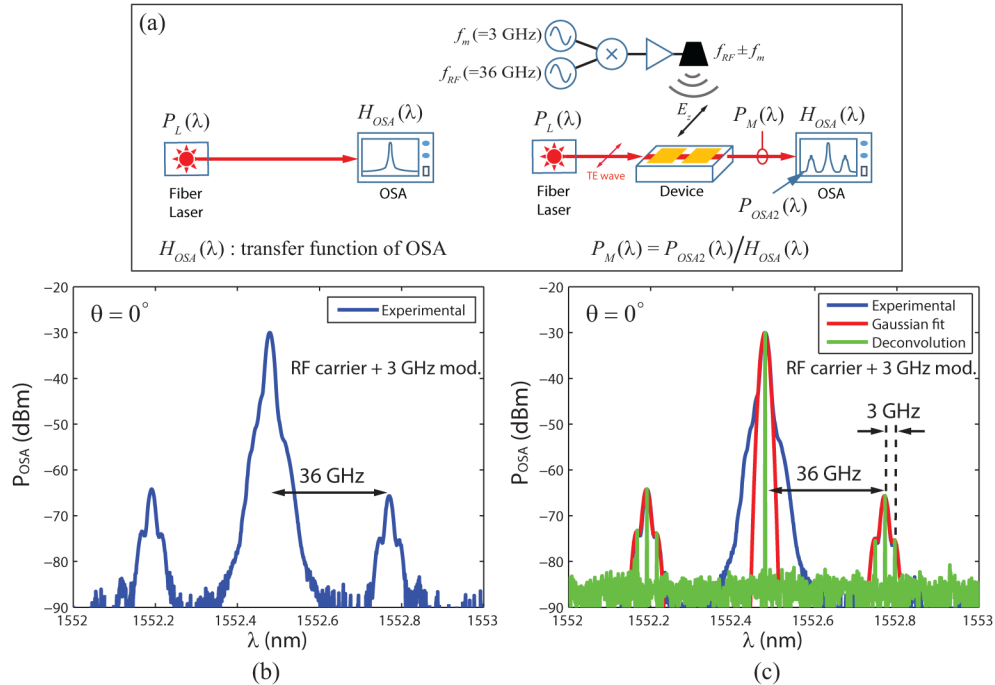


Fig. 7. (a) Schematic showing deconvolution process. “/” means deconvolution. (b) Optical spectrum as a function of optical wavelength and RF frequency when 36 GHz RF carrier and 3 GHz modulation are fed to the horn antenna. (c) Optical spectrum (blue) when RF carrier signal is modulated with 3 GHz sinusoidal signal. The experimental result is fitted to a combination of 7 Gaussian functions (red), which is then deconvolved with the optical spectrum of laser from OSA (transfer function) in order to recover optical carrier, RF carrier, and modulation signal.

5. Conclusions

We have designed and demonstrated an antenna-coupled optical phase modulator based on second-order nonlinear in-plane polymeric waveguide operating at the mm-wave frequency of 37 GHz with CSR of 22 dB under an RF power density of 120 W/m^2 and bandwidth of 2 GHz. We have presented new closed-form expressions for the optical phase modulation in case of both single and array antennas as well as CSR. For thermal, photo, and temporal stabilities, we refer the reader to Ref [25]. and references therein. We believe that this device based on nonlinear polymer shows promise for photonic-based antenna remoting applications. Compared with a typical high speed EOM such as an EOSpace[®] modulator attached to a 0-dBi gain antenna resulting in a $\text{FOM} = 1.75 \text{ W}^{-1/2}$, the FOM of our best device, $2.0 \text{ W}^{-1/2}$, is slightly higher. We couldn't compare our FOM value with other works due to limited system parameters information such as RF and optical power, in their reports. For device improvement, a quasi-phase-matching antenna array structure using push-pull poling may increase the CSR by 6 dB [26]. In addition, unlike Li-based EO crystal, low index nonlinear polymer can be applied to a void nanostructure in order to confine an optical mode in a few hundred nanometer wide slot optical waveguide based on the silicon-on-insulator (SOI) platform, allowing a narrower antenna gap down to $1 \mu\text{m}$ without significant metallic loss [27]. We expect that this will further improve CSR by more than 18 dB compared to $8 \mu\text{m}$ -gap slotted antenna structures. As pointed out in Ref [28], the antenna-to-EO modulator interface is an important research area in need of further development for next generation RF-optical systems that provide low noise figure and large dynamic range [1,2,28,29]. Nonlinear polymers based on second-order nonlinearity are expected to allow high modulation

bandwidth at RF carrier frequencies higher than 100 GHz without significant performance degradation.

Appendix A: Derivation of the optical phase modulation for array of N antenna elements

Here we give details of the derivation of the closed-form expression in Eq. (11) for the RF modulated phase of the optical wave in the case of N antenna elements. Performing the integration in Eq. (10) gives

$$\delta\phi_N(t_0) = \frac{\omega_{op}}{\omega_{RF}} \frac{A}{u} \sum_{s=0}^{N-1} \left\{ \cos \left[k_{RF} u (sL_A + L) - \omega_{RF} t_0 \right] - \cos \left(k_{RF} u s L_A - \omega_{RF} t_0 \right) \right\}. \quad (20)$$

Using the following identity $\cos(x-a) - \cos x = 2 \sin(a/2) \sin(x-a/2)$, this becomes

$$\delta\phi_N(t_0) = 2 \frac{\omega_{op}}{\omega_{RF}} \frac{A}{u} \sin \left(\omega_{RF} \frac{u}{2c} L \right) \sum_{s=0}^{N-1} \sin \left[\omega_{RF} \left(t_0 - s \frac{u}{c} L_A - \frac{u}{2c} L \right) \right], \quad (21)$$

where $x = \omega_{RF} (t_0 - suL_A/c)$ and $a = \omega_{RF} uL/c$. Now using the identity

$$\sum_{s=0}^{N-1} \sin(y - sb) = \frac{\sin \left(\frac{Nb}{2} \right)}{\sin \left(\frac{b}{2} \right)} \sin \left[y - (N-1) \frac{b}{2} \right], \quad (22)$$

we can simplify Eq. (21) to

$$\delta\phi_N(t_0) = 2 \frac{\omega_{op}}{\omega_{RF}} \frac{A}{u} \sin \left(\omega_{RF} \frac{u}{2c} L \right) B_N \sin \left(y - (N-1) \frac{b}{2} \right), \quad (23)$$

where $y = \omega_{RF} (t_0 - uL/2c)$, $b = \omega_{RF} uL_A/c = k_{RF} uL_A$, and the scaling B_N is

$$B_N = \sin \left(\frac{Nb}{2} \right) / \sin \left(\frac{b}{2} \right). \quad (24)$$

Equation (23) with Eq. (24) can then easily be rewritten in the form given in Eq. (11).

Acknowledgments

We thank V. Yun, Y. Leng, and P. Cho for help with the experimental setup, the fabrication, and the data analysis.